Mechanism of Selectivity Control for Zeolites Modified with Organic Monolayers

Xinpei Zhou, John L. Falconer, J. Will Medlin *

Department of Chemical and Biological Engineering, University of Colorado Boulder, Boulder, CO 80309-0596, USA

* Corresponding author.
E-mail address: medlin@colorado.edu (J. Will Medlin).

Abstract

The adsorptive separation of C_3H_6 and C_3H_8 gases using molecular sieves is a challenging process due to the similarity in molecular sizes for the two molecules. In this work, we report that organic phosphonic acid (PA) monolayers on zeolites significantly enhanced the ideal selectivity of C_3H_6/C_3H_8 adsorption by changing the diffusion mechanism based on the properties of the alkyl tail. With an *n*-octadecylphosphonic acid (ODPA) coating on zeolite 5A, the kinetic selectivity of C_3H_6/C_3H_8 was initially >8 at 25 °C, whereas for uncoated 5A, it was limited to ~1.2. Kinetic modelling showed that in ODPA-coated 5A, the diffusion of C_3H_6 and C_3H_8 was limited by the PA monolayer at the external surface of the zeolite. In contrast, for uncoated 5A, it was controlled by the pore channels, so that the enhanced kinetic selectivity from 5A-ODPA was related to a different limiting transport mechanism. The kinetic selectivity was not temperature sensitive in the range of 25–150 °C in 5A-ODPA as the diffusion activation energies of C_3H_6 and C_3H_8 were both small. Modification of 5A with other PAs also increased the kinetic selectivity. Coating with *n*-butylphosphonic acid yielded lower kinetic selectivity than ODPA, ostensibly due to its shorter alkyl tail. Coating with *tert*-butylphosphonic acid, a sterically bulky ligand, decreased kinetic selectivity still further. However, methylphosphonic acid, which partially penetrated the near-surface region of the zeolite, severely lowered the diffusion rates. The use of organic films may enable rational design of selective adsorbents based on providing gas-specific resistance at the pore entrance.

Keywords: Organic phosphonic acid, Self-assembled monolayer, Zeolite, Adsorptive separation, Diffusion mechanism

1. Introduction

Propylene is an important feedstock for a wide variety of products, mainly for polypropylene that is used in packaging films, textile fibers, and other applications. The demand for propylene keeps increasing and currently is over 110 million metric tons annually in the world [1]. The main methods to produce propylene are steam cracking, fluid catalytic cracking, and alkane dehydrogenation, which all result in mixtures of propylene and propane. The mixtures need to be separated to obtain "polymer-grade" propylene (minimum purity of 99.5%) for the manufacture of polypropylene. However, traditional separation processes, especially distillation, are energy intensive. Chemical separations have been reported to account for 10%–15% of the total energy consumption in the United States, and distillation consumes about half of the energy [2]. Cryogenic distillation for the separation of propylene and propane with similar boiling points usually requires towers with 150–200 stages, temperatures of 183–233 K, and pressures of 16–20 bar [3].

In the past several decades, many researchers made efforts at finding alternative processes to improve the separation of propylene and propane, such as adsorption [4–7], absorption [8,9], and membrane separation [10–13]. Among these technologies, adsorptive separation is a promising method with low energy consumption and capital cost. Adsorptive separation can be divided into two main categories: equilibrium separation and kinetic separation. Equilibrium separation is based on the equilibrium loading of one adsorbate being greater than the others, and kinetic separation is by the difference in diffusion rates of adsorbates. Considering the similar kinetic diameters of propylene and propane molecules, rational design of porous adsorbents to achieve high adsorption selectivity is essential for an energy-efficient, kinetic separation process.

Various materials have been studied for the separation of light gases with similar molecular sizes. Carbon molecular sieve fibers with an effective micropore size of 3.4 to 4.9 Å (prepared from pyrolysis of polyvinylidene chloride copolymer) were reported to have propylene/propane (50/50 mixture) adsorptive separation factors of 12–29 [14], but their poor mechanical strength makes them difficult to scale up [3]. Polymeric membranes made from 2,3,5,6-tetra-methyl-1,4-phenylenediamine and 9,10-diisopropyltriptycene-based dianhydride had a propylene/propane ideal selectivity of 16 and a propylene permeability of 817 Barrer [15]. However, polymeric membranes usually cannot simultaneously meet the performance requirements (selectivity 20 and propylene permeability 10 Barrer) [16], and the selectivity usually decreases due to a plasticization effect [3]. Zeolitic imidazolate framework ZIF-8 based membranes have been found to reach propylene/propane selectivity of 100 and propylene permeance $>10^{-8}$ mol Pa^{-1} m^{-2} s^{-1} [17].

Zeolites have been widely investigated for gas separation, owing to their well-defined pores and high chemical, thermal, and mechanical stabilities [18]. There are more than 200 types of zeolites with different structures. To separate gases with similar molecular sizes, zeolites should have appropriate pore openings and channels.

One method to tune the pore structure of zeolites is to change the composition and bulk framework. Grande et al. [19] synthesized lithium-modified zeolite 13X for propylene/propane separation via vacuum pressure swing adsorption and improved the selectivity compared with Na-13X. Shrestha and Dutta [13] used zeolite membranes grown within porous polyethersulfone supports and coated with a thin layer of polydimethoxysilane for propylene/propane separation and found that Ag^+ cation modification improved propylene/propane selectivity from 2.4 to 4.8 and achieved propylene permeability of 10^3 Barrer. Min et al. [20] found that $CaNH_4$-levyne (Si/Al = 15.5 and Fe/Al = 0.27) had an equilibrium ideal selectivity of 11 for propylene/propane

adsorptive separation by the molecular sieve effect of the framework topology and the introduction of Fe to decrease acidity.

For further improving selective adsorption, the external surface of zeolites can be modified with an additional diffusion layer or functional group. Chudasama et al. [21] deposited silica on the external surface of zeolite 4A with tetraethyl orthosilicate and improved the equilibrium ideal selectivity of O_2/N_2 from 0.3 to 2.0 and O_2/Ar from 1.1 to 4.6. Xu et al. [22] deposited monoethanol amine on β-zeolite and improved the ideal selectivity of CO_2/CH_4 from 4.6 to 7.7 and CO_2/N_2 from 12 to 26 based on a steric effect and adsorbate-adsorbent chemical interaction.

Another method is to tune the pore openings of zeolites to improve adsorption selectivity. Dong et al. [23] coated ultrathin microporous TiO_2 on zeolite 5A by combining molecular and atomic layer deposition methods to decrease the pore mouth from 0.8 to 0.6 nm, and the diffusivity ratio of propylene to propane were increased from 1 to 75 and a propylene/propane equilibrium ideal selectivity up to 22 was achieved. Ellis et al. [24] deposited methylphosphonic acid (MPA) self-assembled monolayers (SAMs) on zeolite 5A, and both the initial diffusion rate and apparent uptake of *n*-C_4H_{10} were decreased by >90%; the ideal selectivity of propylene/propane reached 59 ± 14 at 46 kPa.

Modification with PAs is a promising method to tune gas diffusion rates and improve the adsorption selectivity. We have previously characterized PA-modified zeolite 5A with various techniques, including X-ray diffraction (XRD), Brunauer-Emmett-Teller (BET) surface area measurement, inductively coupled plasma-mass spectrometry (ICP-MS), scanning transmission electron microscopy (STEM) with energy-dispersive X-ray spectroscopy (EDS), low energy ion scattering (LEIS), and other methods. It was found that the bulk crystalline structure of zeolites did not change after coating with PAs, and MPA (the smallest PA studied) was located at the near-

surface region of zeolite 5A. All longer-chain PAs were confined to the external surface [24]. Understanding the diffusion mechanism of gas molecules with PA modification may enable rational design of adsorption materials and separation systems. We hypothesized that PA modifiers deposited at the surface can provide an added barrier to the diffusion of C_3H_6 and C_3H_8 into zeolites, and by tuning the properties of PA modifiers, an additional level of control over adsorption selectivity can be achieved. Here, we modified zeolite 5A with different PAs and measured the temperature dependence of the kinetic selectivity in the temperature range of 25 to 150 °C. We then investigated the diffusion mechanism using kinetic models based on a rate-limiting step of internal or surface diffusion.

2. Experimental Methods

2.1. Organic Phosphonic Acid Coating on Zeolite and Characterization

The SAM coating technique developed previously was employed [24]. Zeolite 5A, $Ca_nNa_{12-2n}[(AlO_2)_{12}(SiO_2)_{12}]$ xH_2O (powder, <10 μm, Sigma-Aldrich 233676), was coated with methylphosphonic acid (MPA, ≥97.5%, Alfa Aesar A12619), *n*-butylphosphonic acid (BPA, ≥88.0%, Sigma-Aldrich 737933), *tert*-butylphosphonic acid (TBPA, ≥97.5%, Acros Organics 321520050), and *n*-octadecylphosphonic acid (ODPA, ≥96.0%, Alfa Aesar 20645), respectively. In detail, zeolite 5A (830 mg) was calcined for 4 h in static air at 400 °C, then cooled down close to room temperature and added to a 200-mL solution (0.01 mol/L) of PA in tetrahydrofuran (THF, high-performance liquid chromatography [HPLC] grade, Fisher Chemical T425-4), then stirred for 16 h, and centrifuged at 8000 rpm for 9 min. The supernatant solvent was decanted, and the remaining precipitant was annealed at 120 °C for 6 h, then cooled to room temperature and rinsed with THF four times to remove physisorbed PA. The powder was dried in a vacuum oven at room temperature. To compare the coverage of PAs on BPA- and TBPA-coated zeolite 5A, LEIS

analysis was carried out on a Qtac100 instrument (ION-TOF, Germany) using a 6 keV $^{4+}$He beam. Five to eight spectra were taken from each sample, and the smoothed curve was obtained by taking the average of these spectra, subtracting a linear background, and smoothing. The elemental composition from LEIS was determined by integrating the area under the detected peaks.

2.2. Pressure-Decay Adsorption Measurement

The pressure-decay measurement was performed on an Autosorb-1 apparatus (Quantachrome Instruments) equipped with a custom LabVIEW-based data acquisition system. Before each measurement, the sample (100 mg) was pretreated for 3 h at 200 °C under vacuum. Three gases, CO_2 (≥99.999%, Airgas), C_3H_6 (≥99.5%, Airgas), and C_3H_8 (≥99.5%, Airgas), were tested separately at a manifold pressure of 40 kPa and room temperature for uncoated zeolite 5A and the zeolites coated with MPA, BPA, TBPA, and ODPA, respectively. Based on the pressure drop during adsorption, the amount of adsorbed gas and ideal selectivity (ratio of C_3H_6 uptake to C_3H_8 uptake at the same adsorption time and temperature) were calculated. To investigate the effect of temperature on the ideal selectivity of C_3H_6/C_3H_8, the adsorption was measured in the temperature range of 25 to 150 °C.

2.3. Diffusion Models

Kinetic models describing uptake limited by internal or surface diffusion were used to simulate adsorption process of porous adsorbents under the assumptions of uniform particle size, spherical particle shape, and constant adsorbate concentration on the surface of adsorbent. In the internal diffusion model, the uptake is controlled entirely by internal diffusion, and the surface resistance is assumed to be negligible. The equation is expressed as the following [25].

$$\frac{m_t}{m_\infty} = 1 - \frac{6}{\pi^2}\sum_{n=1}^{\infty}\frac{1}{n^2}e^{-n^2\pi^2 t(D/R^2)} \quad (1)$$

In the surface limitation model, the uptake is assumed to be controlled entirely by surface resistance. The equation is expressed as the following [26].

$$\frac{m_t}{m_\infty} = 1 - e^{-3t(k/R)} \quad (2)$$

In Eq. (1) and (2), m_t/m_∞ is the ratio of mass adsorbed at time t to that at infinite time, R is equivalent radius of pores in adsorbent, D is intrapore diffusivity, and k is surface rate coefficient. We carried out nonlinear regression (minimizing the residual sum of squares) for full experimental data of m_t versus t (120 min for C_3H_6 and C_3H_8 adsorption on ODPA-coated 5A and C_3H_6 adsorption on MPA-coated 5A, and 10 min for the others) to find the model parameters (D/R^2 in internal diffusion and k/R in surface limitation model) and the loadings at infinite adsorption time. To investigate the sensitivity of the fits to the time used for fitting, the loadings at long times from use of the entire experimental time for the fits was used to calculate the fractional uptakes m_t/m_∞, then m_t/m_∞ versus t was fit for various time spans.

The diffusion rate constants evaluated at different temperatures were used to calculate activation energies. Plots of ln K versus $1/T$ were employed to determine the apparent activation energies E_a of gas adsorption, in which K is the diffusion rate constant (D/R^2 for internal diffusion model and k/R for surface limitation model), and T is the absolute temperature.

2.4 Thermodynamic Calculations

Plots of ln $[((p_i - p_e)/p^0)/(p_e/p^0)]$ versus $1/T$ based on the van't Hoff equation were used to determine the standard enthalpy changes ΔH^0 and standard entropy changes ΔS^0 of gas adsorption in our system, in which p_i is the initial pressure of the system, p_e is the equilibrium pressure of the system, p^0 is the standard pressure (100 kPa), and T is the absolute temperature.

3. Results and Discussion

3.1. Organic Phosphonic Acids Tune Gas Adsorption Rates in Zeolite 5A

Pressure-decay adsorption profiles of gases CO_2, C_3H_6, and C_3H_8 on uncoated zeolite 5A and the 5A coated with PAs (TBPA, BPA, ODPA, and MPA) at 25 °C are shown in Figs. 1 and S1. On uncoated 5A at 25 °C, the adsorption equilibrium loadings of these three gases measured from highest to lowest were: CO_2 (2.40 mmol/g) > C_3H_6 (1.85 mmol/g) > C_3H_8 (1.48 mmol/g). The highest loading of CO_2 could be attributed to its small molecular kinetic diameter (where the kinetic diameters were reported as 3.3 Å for CO_2 [27], 4.31 Å for C_3H_6 [28], and 4.46 Å for C_3H_8 [28]), linear geometry, and strong interaction forces [29, 30]. The lowest loading of C_3H_8 was mainly ascribed to its molecular size [30].

The PAs had minimal effect on CO_2 adsorption, but they decreased the adsorption rates of C_3H_6 and C_3H_8. The adsorption from fastest to slowest for both C_3H_6 and C_3H_8 was: 5A > 5A-TBPA > 5A-BPA > 5A-ODPA >> 5A-MPA. For C_3H_6, the approximate time to reach equilibrium loading was 1 min on uncoated 5A, 2 min on TBPA-coated 5A, 10 min on BPA-coated 5A, 20 min on ODPA-coated 5A, and >120 min on MPA-coated 5A. With PA coatings, the adsorption rate of C_3H_8 decreased even more; the time to reach equilibrium was 1 min on uncoated 5A, 8 min on TBPA-coated 5A, 80 min on BPA-coated 5A, 100 min on ODPA-coated 5A, and >>120 min on MPA-coated 5A.

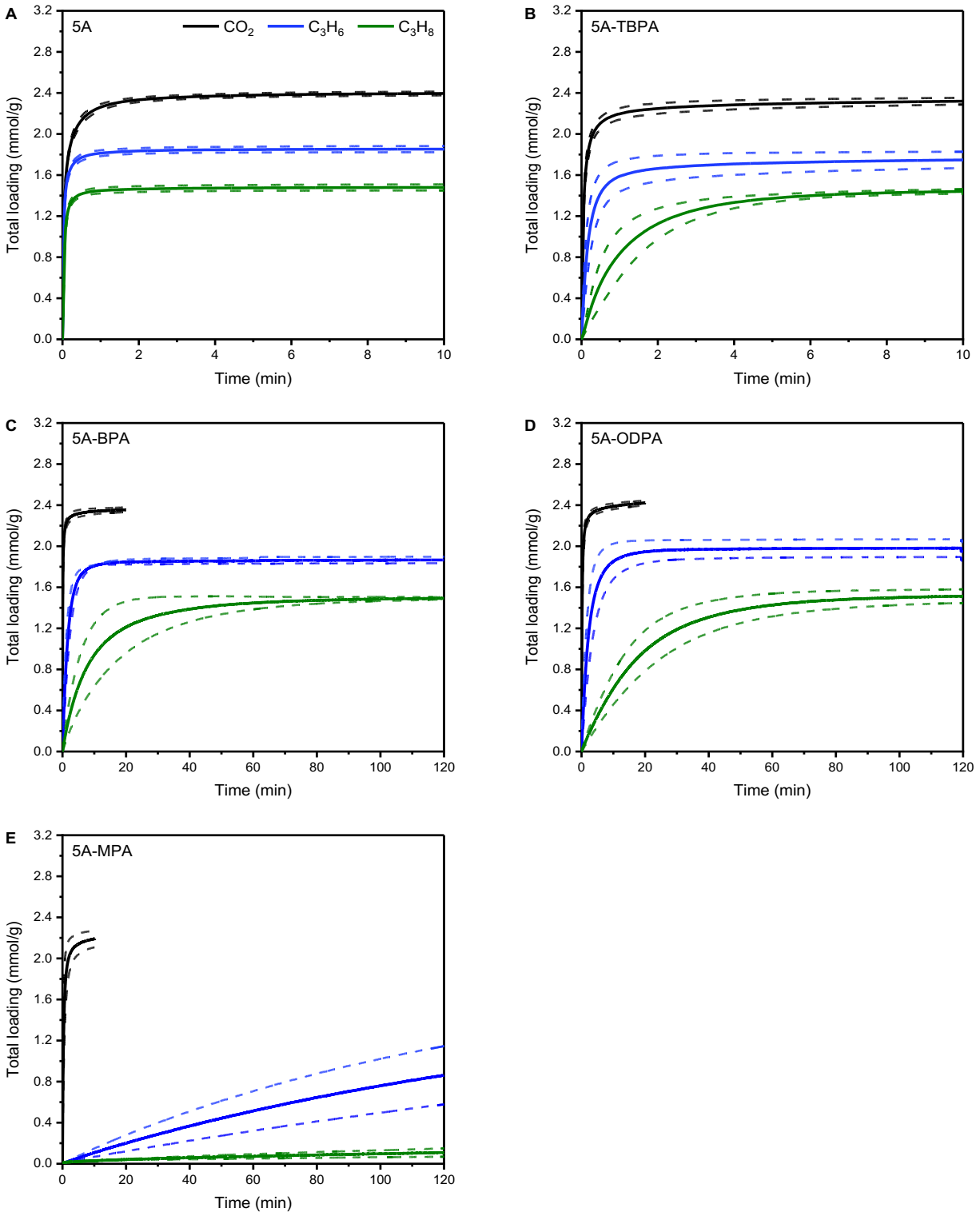

Fig. 1. CO_2, C_3H_6, and C_3H_8 adsorption on (A) uncoated, (B) TBPA-, (C) BPA-, (D) ODPA-, and (E) MPA-coated 5A at 25 °C. Uncertainty bounds are based on standard deviations of triplicate measurements for separately prepared samples, with the exception of C_3H_6 and

C_3H_8 adsorption on 5A-MPA, where the dashed curves represent the span of duplicate measurements with separate samples.

The chain length and steric configuration of PA modifiers affected the diffusion rates of both C_3H_6 and C_3H_8. Deposition of MPA, which partially penetrated the near-surface region of zeolite based on the elemental analysis on different regions of the particle with EDS and surface element detection with LEIS [24], severely lowered the diffusion rates. The PAs with longer alkyl chains, BPA and ODPA, which were confined to a monolayer on the external surface of zeolite [24], had less resistance to gas diffusion than MPA, and ODPA (with a longer alkyl chain) slowed diffusion more than BPA. Moreover, TBPA, a sterically bulkier modifier, had lower PA coverage than BPA (with a linear alkyl chain) on the surface of zeolite 5A particles based on LEIS analysis (Fig. S2 and Table S1), and it had less effect on diffusion rates than BPA. Ellis et al. [24] also found that PA chain length had a similar effect on initial diffusion rates of gases, where they used CO_2, CH_4, and *n*-C_4H_{10} for the measurements; however, they did not investigate sterically bulky modifiers.

The effect of PA coatings on ideal selectivity of C_3H_6/C_3H_8 adsorption at 25 °C is shown in Fig. 2. Before adsorption reached equilibrium, the kinetic selectivities of C_3H_6/C_3H_8 on TBPA-, BPA-, and ODPA-coated 5A were higher than uncoated 5A, and the kinetic selectivities for the coatings from highest to lowest were: ODPA > BPA > TBPA. The adsorbents with higher kinetic selectivities took longer time to reach equilibrium selectivity. For ODPA-coated 5A, the kinetic selectivity was initially >8, and it reached stability after 80 min. For MPA-coated 5A, the kinetic selectivity was about 7 after ~60 min (data before 30 min were error-prone due to the low uptakes of C_3H_6 and C_3H_8), but C_3H_6 loading was low (0.86 mmol/g at 120 min).

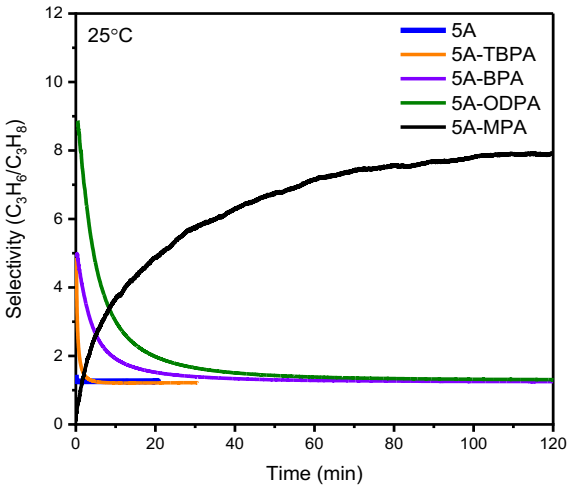

Fig. 2. C_3H_6/C_3H_8 ideal selectivities as a function of adsorption time on uncoated, TBPA-, BPA-, ODPA-, and MPA-coated 5A at 25 °C.

In summary, modification of zeolite 5A with PAs can tune the diffusion rates of C_3H_6 and C_3H_8. The high kinetic selectivity of C_3H_6/C_3H_8 adsorption from PA-coated 5A at short times could potentially be used for kinetic separation of C_3H_6 and C_3H_8, especially in the case of ODPA-coated 5A, which had an initial ideal selectivity >8 under the reported experimental conditions.

3.2. Temperature Dependence of Equilibrium and Kinetic Adsorption on PA-coated 5A

The temperature dependence of C_3H_6, C_3H_8, and CO_2 adsorption in the temperature range of 25 to 150 °C on uncoated, ODPA-coated, and MPA-coated 5A is shown in Figs. 3 and S3. We selected ODPA and MPA coatings for these variable temperature studies to probe the effects of surface-confined and surface-penetrating coatings, respectively. At higher temperatures, C_3H_6, C_3H_8, and CO_2 had lower equilibrium loadings on all adsorbents, as expected for exothermic adsorption processes, and C_3H_8 had a greater decrease in equilibrium loading than C_3H_6. With the increase of temperature, the gases required less time to reach adsorption equilibrium on uncoated and ODPA-coated 5A. For MPA-coated 5A, C_3H_6 and C_3H_8 still had not reached equilibrium after 120 min at 150 °C.

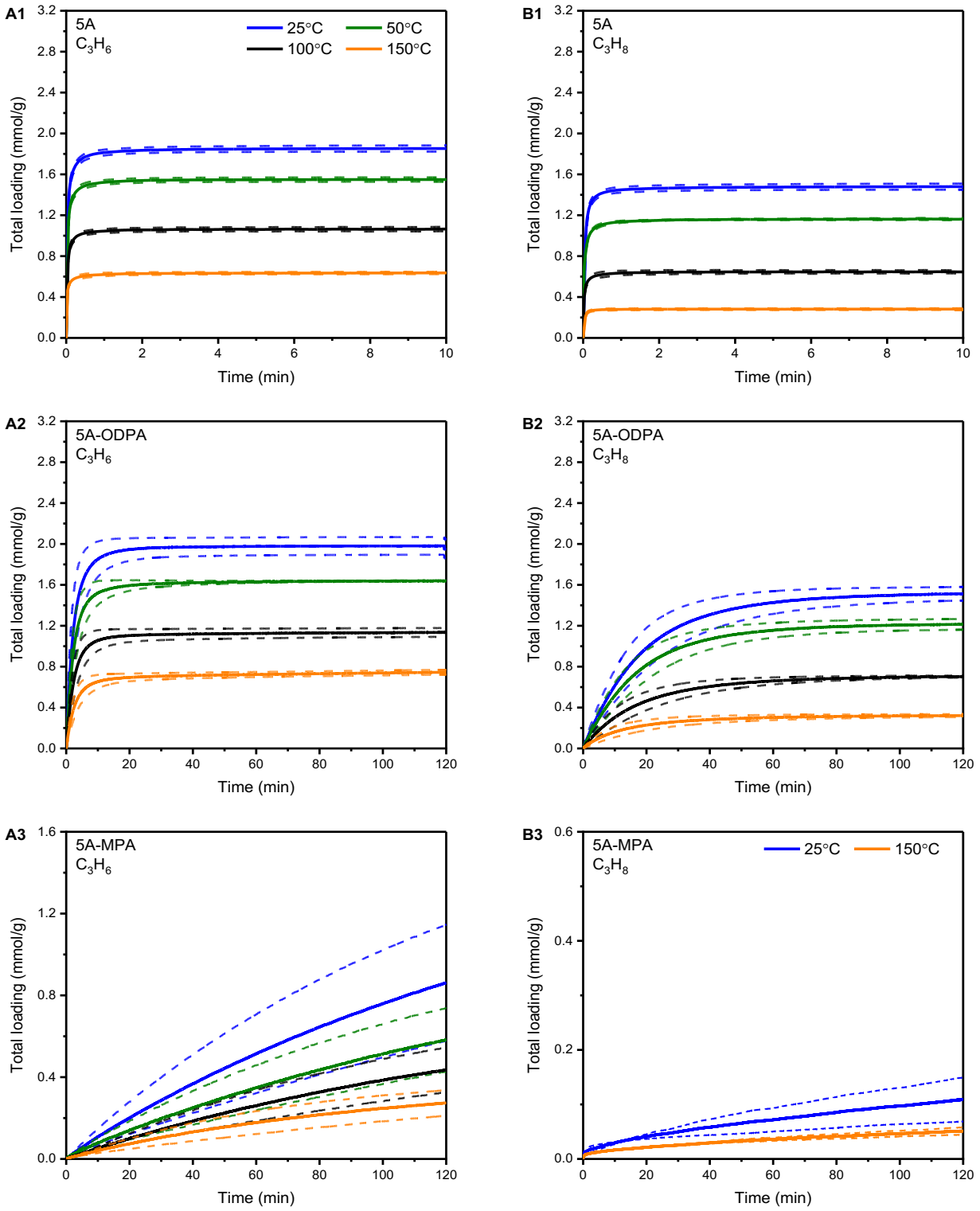

Fig. 3. Temperature dependence (25–150 °C) of C_3H_6 (A1, A2, and A3) and C_3H_8 (B1, B2, and B3) adsorption on uncoated, ODPA-, and MPA-coated 5A. Uncertainty bounds are generally based on standard deviations of triplicates for separately prepared samples, with

the exception of C_3H_6 and C_3H_8 adsorption on 5A-MPA, where the dashed curves represent the span of duplicates.

The equilibrium selectivity of C_3H_6/C_3H_8 adsorption increased as the temperature increased from 25 to 150 °C on both uncoated and ODPA-coated 5A, as shown in Fig. 4. For uncoated 5A, selectivity was nearly constant with time at all temperatures, and the equilibrium selectivity was below 2.4 even at 150 °C (Fig. 4A). For ODPA-coated 5A, the kinetic selectivity was initially >8 and then decreased with time at all temperatures (Fig. 4B). After the adsorption approached equilibrium, the equilibrium selectivity was similar to that for uncoated 5A at the same temperature. The temperature influence on the initial selectivity was not strong, so that kinetic selectivity was less sensitive to temperature than equilibrium selectivity.

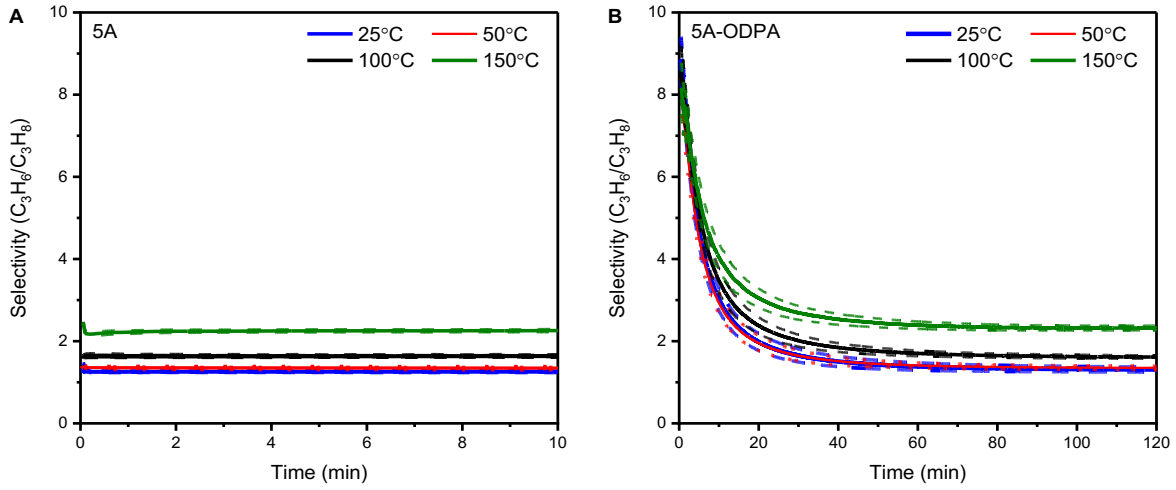

Fig. 4. C_3H_6/C_3H_8 ideal selectivities as a function of temperature and time on (A) uncoated and (B) ODPA-coated 5A. The dashed curves represent the uncertainty bounds based on standard deviations of triplicates for separately prepared samples.

Based on the temperature-dependent equilibrium loading data, the standard enthalpy changes ΔH^0 and standard entropy changes ΔS^0 of C_3H_6, C_3H_8 and CO_2 adsorption on zeolite 5A were calculated (Table 1) from plots of $\ln [((p_i - p_e)/p^0)/(p_e/p^0)]$ versus $1/T$ (Fig. S4). The enthalpy changes ΔH^0 of adsorption was more negative for C_3H_8 than C_3H_6, with a difference (ΔH^0_{C3H8} −

ΔH^0_{C3H6}) of -4.1 kJ/mol, so rising temperature was found to disfavor the adsorption of C_3H_8 and result in higher equilibrium selectivity (Fig. 4A). Adsorption of CO_2 had a more negative enthalpy than C_3H_6 and C_3H_8, so its equilibrium loading was more sensitive to temperature, as shown in Figs. S3, 3A1, and 3B1. The small enthalpy changes for C_3H_6, C_3H_8 and CO_2 adsorption on zeolite 5A are in favor of energy management of the process and the regeneration of adsorbent.

Table 1 Standard enthalpy changes ΔH^0 and standard entropy changes ΔS^0 of C_3H_6, C_3H_8, and CO_2 adsorption on uncoated zeolite 5A.

5A	C_3H_6	C_3H_8	CO_2
ΔH^0 (kJ/mol)	-12.1 ± 0.5	-16.2 ± 0.5	-29.5 ± 1.0
ΔS^0 (J/mol·K)	-35.1 ± 1.4	-52.9 ± 1.6	-85.5 ± 2.7

3.3. Diffusion Modeling of Kinetic Adsorption

To determine the rate-limiting resistance of gas diffusion into zeolite 5A coated with PAs, gas adsorption measured in the temperature range of 25 to 150 °C was simulated using an internal diffusion model and a surface limitation model. The fitting was appraised using the adjusted R^2, where the model with a higher adjusted R^2 would be a better fit. For instance, C_3H_6 adsorption on MPA-coated 5A in the temperature range of 25 to 150 °C had adjusted R^2 in the range of 0.86–0.88 from internal diffusion model while they were all nearly 1 from surface limitation model (Table S10). Therefore, the surface limitation model was a better fit than the internal diffusion model in this case. On uncoated 5A for CO_2, C_3H_6, and C_3H_8 adsorption, the internal diffusion model resulted in higher adjusted R^2values and so fit better than the surface limitation model (Figs. 5A and S6–S8, Tables S3–S5). For ODPA- and MPA-coated 5A, the internal diffusion model still provided a better fit for CO_2 adsorption, but the surface limitation model was a much better fit for C_3H_6 adsorption on 5A-ODPA and 5A-MPA and also for C_3H_8 adsorption on 5A-ODPA (Figs. 5B and S9–S13, Tables S6–S10). The simulation of C_3H_8 adsorption on 5A-MPA was not conducted since the uptake was low, only 0.15 mmol/g after 120 min, so that it had a big relative error. The

observation of surface limitation in the case of the PA-modified zeolites was intuitive given that: (1) previous work had shown that PAs were confined to the surface of the zeolites [24]; and (2) the observations in the current work showed that PAs drastically changed adsorption rates and selectivities. In addition, for adsorption with relatively fast diffusion rates, including C_3H_6 and C_3H_8 adsorption on uncoated 5A and CO_2 adsorption on uncoated 5A and PA-coated 5A, the fitting curves from both models deviated from experimental data at the inflection points of the curves, especially for CO_2 adsorption on uncoated 5A. We tested the effect of using different time scales for the fits; here, longer times provide more emphasis to the final equilibration process, whereas shorter times emphasize the initial rise in uptake to a greater extent. In particular, models for adsorption times near the inflection points (0.2, 0.5, and 1 min) were studied; although the fits in all cases showed some deviation from experiment, the internal diffusion model was always superior to surface limitation model for CO_2 adsorption on uncoated 5A (Table S11).

With PA modification, the dominant diffusion resistance for C_3H_6 and C_3H_8 changed such that the surface penetration model clearly provided the better fit. We proposed that PAs functioned as "gate-keepers" by adding an additional diffusion barrier to gas adsorption (through the presence of an organic film that restricted access to the pore opening) and decreasing the diffusion rate more for C_3H_8 than C_3H_6. The PA modifiers decreased the diffusion rates of C_3H_6 and C_3H_8, and MPA had more influence than ODPA. According to the diffusion models, the notion that the effects of ODPA, BPA, and TBPA modification would improve kinetic selectivity through adding a surface resistance layer was also consistent with the similar equilibrium selectivity observed for those coatings and the uncoated zeolite.

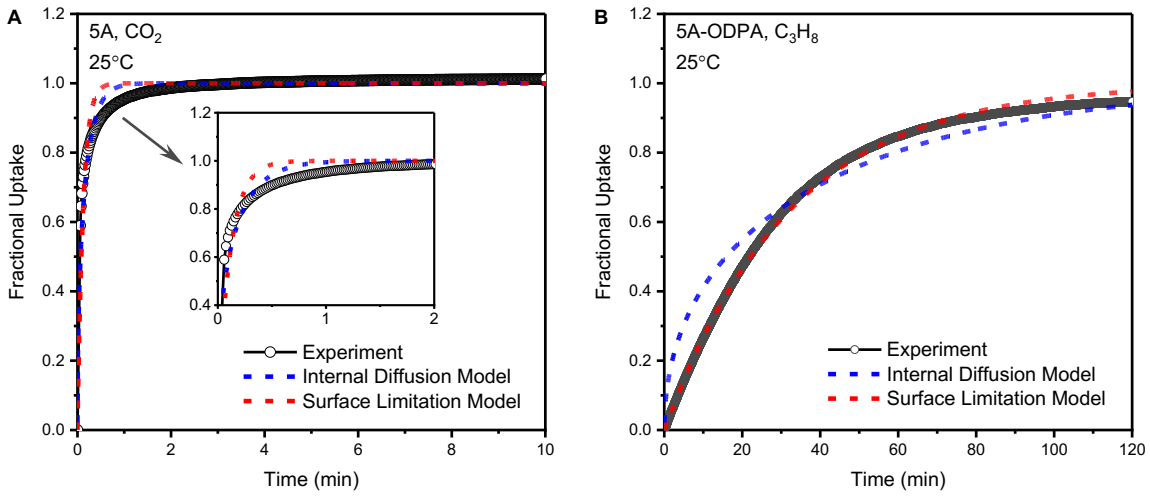

Fig. 5. Modeling of uptake curves for (A) CO_2 on uncoated and (B) C_3H_8 on ODPA-coated 5A at 25 °C.

Based on the diffusion rate constants K in the temperature range of 25 to 150 °C, plots of ln K versus $1/T$ (Fig. S5) were generated, and the apparent activation energies E_a of C_3H_6, C_3H_8 and CO_2 were determined as listed in Table 2. The activation energy is related to the enthalpy barrier for gas molecules to diffuse into zeolites in the adsorption process. In uncoated, ODPA-, and MPA-coated 5A, the diffusion enthalpy barrier for CO_2 was higher than C_3H_6, i.e. CO_2 diffusion was more sensitive to temperature despite being a smaller molecule. In ODPA-coated 5A, the apparent activation energies of C_3H_6 and C_3H_8 were small and of a similar magnitude, so that the initial selectivity was essentially temperature insensitive (Fig. 4B). The standard deviation of activation energy for CO_2 adsorption was greater, which was ascribed to the CO_2 adsorption rate being fast, such that fewer data points could be obtained before equilibration. Though, the activation energy of CO_2 adsorption on uncoated 5A was not significantly affected by the time span employed for the modelling (Table S11).

Although we can conclude long-chain PA coatings function by adding a diffusion resistance that differs for different gases, the precise mechanism for selective suppression of C_3H_8 diffusion is not clear. Based on the higher diffusion rates for both C_3H_6 and C_3H_8 on the BPA-

coated zeolite than the ODPA-coated, we proposed that diffusion was controlled in part by the thickness of the organic layer. Interestingly, the difference in diffusion rates for C_3H_6 and C_3H_8 in ODPA-coated 5A appeared to be largely entropically driven, i.e. there was a significant difference in pre-exponential factors (Table S2) rather than activation energies in the Arrhenius analysis. Thus, the more rapid diffusion of C_3H_6 through ODPA might be driven by a larger number of available configurations in the closely packed monolayer film. Molecular dynamics simulations may be needed to provide molecular insights into the diffusion pathways available for different gases in these organic films.

Table 2 Apparent activation energies (determined by Arrhenius analysis of fitted rate parameters) of C_3H_6, C_3H_8, and CO_2 adsorption on uncoated, ODPA-, and MPA-coated 5A.

Adsorbate	E_a (kJ/mol)		
	5A	5A-ODPA	5A-MPA
C_3H_6	1.8 ± 0.4	1.0 ± 0.2	0.5 ± 0.1 [a]
C_3H_8	3.6 ± 0.2	2.2 ± 0.2	/ [b]
CO_2	9.8 ± 1.1	9.7 ± 1.8	7.4 ± 1.0

* The surface limitation model was employed for C_3H_6 and C_3H_8 adsorption on PA-coated 5A, and the internal diffusion model for the others.
[a] From duplicate measurement, and the others from triplicates.
[b] The loadings of C_3H_8 on MPA-coated 5A at 25 and 150 °C were both small, and consequently its activation energy was not determined.

Coatings of PAs on the surface of zeolites changed the dominant diffusion barrier for gas molecules from pore channels to coating layers, thereby improving the kinetic selectivity of C_3H_6 over C_3H_8 by preferentially decreasing the diffusion rate of C_3H_8. Moreover, the diffusion rates (and thus kinetic selectivities) of gases can apparently be controlled by varying the structure of PAs, including parameters such as alkyl chain length and steric configuration. Other structural variations (e.g., incorporation of unsaturated groups or heteroatoms) could lead to further ability to tune kinetic adsorption rates. The ideal selectivity of C_3H_6/C_3H_8 adsorption was investigated in this work, but further measurements are needed for gas mixture separation with PA-coated zeolites

for practical application. Compared with the approaches to modify the bulk structure of zeolites for gas separation, this approach has potential to provide another lever to tune the diffusion rates of gases by choosing suitable PAs and zeolites. Such an approach may be broadly applicable to diverse adsorbents, i.e., a kinetically selective coating can enhance performance for an underlying equilibrium-selective material.

4. Conclusions

Modification of zeolite 5A with PAs was shown to increase the diffusion resistance of C_3H_6 and C_3H_8, which changed the rate-limiting step from internal diffusion to surface penetration and provided a basis for kinetic separation. For both uncoated and ODPA-coated 5A, the equilibrium selectivity of C_3H_6/C_3H_8 adsorption increased when rising temperature, and the kinetic selectivity was less sensitive to temperature than equilibrium selectivity. The modifier ODPA (with a longer alkyl chain) decreased the diffusion rates of C_3H_6 and C_3H_8 more than BPA (with a shorter alkyl chain), and TBPA (with a sterically bulkier configuration) had the least effect on diffusion rates. The zeolite 5A coated with ODPA had an initial ideal selectivity of C_3H_6/C_3H_8 adsorption >8, and it had higher kinetic selectivity than uncoated 5A within 80 min, making it potentially attractive for efficient adsorptive separation of C_3H_6 and C_3H_8.

CRediT authorship contribution statement

Xinpei Zhou: Investigation, Visualization, Writing – Original draft. **John L. Falconer:** Conceptualization, Methodology, Writing – Review & Editing. **J. Will Medlin:** Supervision, Conceptualization, Methodology, Funding acquisition, Writing – Review & Editing.

Declarations of Interest

The authors declare that they have no known competing financial interests or personal relationships that could have appeared to influence the work reported in this paper.

Acknowledgments

This work was supported by the National Science Foundation [grant CBET 1916738]. We acknowledge Dr. Sadegh Yazdi of University of Colorado Boulder for carrying out the LEIS measurements. Support from the Facility for Electron Microscopy of Materials at the University of Colorado at Boulder (CU FEMM, RRID: SCR_019306) is acknowledged.

References

[1] A. Akah, M. Al-Ghrami, Maximizing propylene production via FCC technology, Appl. Petrochem. Res. 5 (2015) 377–392. https://doi.org/10.1007/s13203-015-0104-3.

[2] D.S. Sholl, R.P. Lively, Seven chemical separations to change the world, Nature. 532 (2016) 435–437. https://doi.org/10.1038/532435a.

[3] R. Faiz, K. Li, Polymeric membranes for light olefin/paraffin separation, Desalination. 287 (2012) 82–97. https://doi.org/10.1016/j.desal.2011.11.019.

[4] F.A. Da Silva, A.E. Rodrigues, Vacuum swing adsorption for propylene/propane separation with 4A zeolite, Ind. Eng. Chem. Res. 40 (2001) 5758–5774. https://doi.org/10.1021/ie0008732.

[5] H. Maghsoudi, H. Abdi, A. Aidani, Temperature- and pressure-dependent adsorption equilibria and diffusivities of propylene and propane in pure-silica Si-CHA zeolite, Ind. Eng. Chem. Res. 59 (2020) 1682–1692. https://doi.org/10.1021/acs.iecr.9b05451.

[6] L. Li, R.-B. Lin, R. Krishna, X. Wang, B. Li, H. Wu, J. Li, W. Zhou, B. Chen, Flexible-robust metal-organic framework for efficient removal of propyne from propylene, J. Am. Chem. Soc. 139 (2017) 7733–7736. https://doi.org/10.1021/jacs.7b04268.

[7] M.H. Weston, Y.J. Colón, Y.S. Bae, S.J. Garibay, R.Q. Snurr, O.K. Farha, J.T. Hupp, S.T. Nguyen, High propylene/propane adsorption selectivity in a copper(catecholate)-decorated porous organic polymer, J. Mater. Chem. A. 2 (2014) 299–302. https://doi.org/10.1039/C3TA12999C.

[8] A. Ortiz, L.M. Galán, D. Gorri, A.B. de Haan, I. Ortiz, Reactive ionic liquid media for the separation of propylene/propane gaseous mixtures, Ind. Eng. Chem. Res. 49 (2010) 7227–7233. https://doi.org/10.1021/ie100576r.

[9] G. Yu, L. Deng, A.A. Abdeltawab, S.S. Al-Deyab, X. Chen, J. Zhang, Functional solution composed of Cu(I) salt and ionic liquids to separate propylene from propane, Ind. Eng. Chem. Res. 53 (2014) 13430–13435. https://doi.org/10.1021/ie501522m.

[10] S. Kasahara, E. Kamio, R. Minami, H. Matsuyama, A facilitated transport ion-gel membrane for propylene/propane separation using silver ion as a carrier, J. Membr. Sci. 431 (2013) 121–130. https://doi.org/10.1016/j.memsci.2012.12.026.

[11] M.L. Chng, Y. Xiao, T.-S. Chung, M. Toriida, S. Tamai, Enhanced propylene/propane separation by carbonaceous membrane derived from poly (aryl ether ketone)/2,6-bis(4-azidobenzylidene)-4-methyl-cyclohexanone interpenetrating network, Carbon. 47 (2009) 1857–1866. https://doi.org/10.1016/j.carbon.2009.03.032.

[12] Y. Pan, T. Li, G. Lestari, Z. Lai, Effective separation of propylene/propane binary mixtures by ZIF-8 membranes, J. Membr. Sci. 390–391 (2012) 93–98. https://doi.org/10.1016/j.memsci.2011.11.024.

[13] S. Shrestha, P.K. Dutta, Modification of a continuous zeolite membrane grown within porous polyethersulfone with Ag(I) cations for enhanced propylene/propane gas separation, Microporous Mesoporous Mater. 279 (2019) 178–185. https://doi.org/10.1016/j.micromeso.2018.12.032.

[14] J. Liu, J. Goss, T. Calverley, Y. Liu, C. Broomall, J. Kang, R. Golombeski, D. Anaya, B. Moe, K. Mabe, G. Watson, A. Wetzel, Carbon molecular sieve fiber with 3.4–4.9 angstrom effective micropores for propylene/propane and other gas separations, Microporous Mesoporous Mater. 305 (2020) 110341. https://doi.org/10.1016/j.micromeso.2020.110341.

[15] R.J. Swaidan, B. Ghanem, R. Swaidan, E. Litwiller, I. Pinnau, Pure- and mixed-gas propylene/propane permeation properties of spiro- and triptycene-based microporous polyimides, J. Membr. Sci. 492 (2015) 116–122. https://doi.org/10.1016/j.memsci.2015.05.044.
[16] M. Guo, M. Kanezashi, Recent progress in a membrane-based technique for propylene/propane separation, Membranes. 11 (2021) 310. https://doi.org/10.3390/membranes11050310.
[17] X. Ma, P. Kumar, N. Mittal, A. Khlyustova, P. Daoutidis, K.A. Mkhoyan, M. Tsapatsis, Zeolitic imidazolate framework membranes made by ligand-induced permselectivation, Science. 361 (2018) 1008–1011. https://doi.org/10.1126/science.aat4123.
[18] Y. Li, L. Li, J. Yu, Applications of zeolites in sustainable chemistry, Chem. 3 (2017) 928–949. https://doi.org/10.1016/j.chempr.2017.10.009.
[19] C.A. Grande, J. Gascon, F. Kapteijn, A.E. Rodrigues, Propane/propylene separation with Li-exchanged zeolite 13X, Chem. Eng. J. 160 (2010) 207–214. https://doi.org/10.1016/j.cej.2010.03.044.
[20] J.G. Min, K.C. Kemp, S.B. Hong, Propylene/propane separation on a ferroaluminosilicate levyne zeolite, Microporous Mesoporous Mater. 294 (2020) 109833. https://doi.org/10.1016/j.micromeso.2019.109833.
[21] C.D. Chudasama, J. Sebastian, R.V. Jasra, Pore-size engineering of zeolite A for the size/shape selective molecular separation, Ind. Eng. Chem. Res. 44 (2005) 1780–1786. https://doi.org/10.1021/ie049333l.
[22] X. Xu, X. Zhao, L. Sun, X. Liu, Adsorption separation of carbon dioxide, methane and nitrogen on monoethanol amine modified β-zeolite, J. Nat. Gas Chem. 18 (2009) 167–172. https://doi.org/10.1016/S1003-9953(08)60098-5.
[23] Q. Dong, Z. Song, F. Zhou, H. Li, M. Yu, Ultrathin, fine-tuned microporous coating modified 5A zeolite for propane/propylene adsorptive separation, Microporous Mesoporous Mater. 281 (2019) 9–14. https://doi.org/10.1016/j.micromeso.2019.02.038.
[24] L.D. Ellis, S.T. Parker, J. Hu, S.F. Zaccarine, M.J. Stellato, H.H. Funke, C. Sievers, S. Pylypenko, J.L. Falconer, J.W. Medlin, Tuning gas adsorption selectivity and diffusion rates in zeolites with phosphonic acid monolayers, Cell Rep. Phys. Sci. 1 (2020) 100036. https://doi.org/10.1016/j.xcrp.2020.100036.
[25] H. Abdi, H. Maghsoudi, All-silica DD3R zeolite for adsorptive separation of propylene from propane: Equilibrium and kinetic data, Microporous Mesoporous Mater. 307 (2020) 110513. https://doi.org/10.1016/j.micromeso.2020.110513.
[26] D.M. Ruthven, Diffusion in type A zeolites: New insights from old data, Microporous Mesoporous Mater. 162 (2012) 69–79. https://doi.org/10.1016/j.micromeso.2011.12.025.
[27] O. Cheung, N. Hedin, Zeolites and related sorbents with narrow pores for CO_2 separation from flue gas, RSC Adv. 4 (2014) 14480–14494. https://doi.org/10.1039/C3RA48052F.
[28] W. Zhu, F. Kapteijn, J.A. Moulijn, Shape selectivity in the adsorption of propane/propene on the all-silica DD3R, Chem. Commun. (1999) 2453–2454. https://doi.org/10.1039/a906465f.
[29] M. Gehre, Z. Guo, G. Rothenberg, S. Tanase, Sustainable separations of C_4-hydrocarbons by using microporous materials, ChemSusChem. 10 (2017) 3947–3963. https://doi.org/10.1002/cssc.201700657.

[30] T.D. Pham, R.F. Lobo, Adsorption equilibria of CO_2 and small hydrocarbons in AEI-, CHA-, STT-, and RRO-type siliceous zeolites, Microporous Mesoporous Mater. 236 (2016) 100–108. http://dx.doi.org/10.1016/j.micromeso.2016.08.025.